Journal of Alloys and Compounds 509 (2011) 6123–6129

Contents lists available at ScienceDirect

Journal of Alloys and Compounds

journal homepage: www.elsevier.com/locate/jallcom

The bending strength temperature dependence of the directionally solidified eutectic LaB_6–ZrB_2 composite

I. Bogomol[a,b,*], T. Nishimura[b], Yu. Nesterenko[a], O. Vasylkiv[b], Y. Sakka[b], P. Loboda[a]

[a] National Technical University of Ukraine "KPI", Peremogy av. 37, Kyiv 03056, Ukraine
[b] Nano Ceramics Center, National Institute for Materials Science, 1-2-1, Sengen, Tsukuba, Ibaraki 305-0047, Japan

ARTICLE INFO

Article history:
Received 26 January 2011
Accepted 17 February 2011
Available online 16 March 2011

Keywords:
Directionally solidified eutectic
Ceramic composites
Lanthanum hexaboride
Zirconium diboride
Bending strength

ABSTRACT

A directionally solidified LaB_6–ZrB_2 eutectic was prepared by the floating zone method based on the crucible-free zone melting of compacted powders. ZrB_2 and LaB_6 powders were used as the initial materials. The bending strength of the composite was evaluated in the temperature range of 25–1600 °C and reached 950 MPa at 1600 °C. Using a residual stress analysis, fracture toughness, and SEM and TEM fracture investigations, the toughening mechanisms under different conditions were studied. We speculate that the strength of the LaB_6–ZrB_2 eutectic at 25–1200 °C is mainly associated with crack deflection, bridge toughening mechanisms and increasing plasticity of the ZrB_2 phase; and at 1200–1600 °C, with the increasing plasticity of the matrix and fibers. By analyzing the dislocation structure of the fibers, the occurrence of strain hardening in the single crystalline ZrB_2 during high-temperature deformation was revealed. The change from the brittle to ductile fracture mode for the directionally solidified LaB_6–ZrB_2 eutectic at near 1600 °C was determined.

1. Introduction

Lanthanum hexaboride is widely used as high-performance electron source with high brightness and longevity, low work function and high chemical stability [1–4]. However, the applications of LaB_6 are rather limited due to its severe brittleness and hard machining [5].

Ceramic directionally solidified eutectics have attracted considerable attention because of their thermodynamic compatibility and microstructural stability up to very high temperature [6]. In works [5,7,8] it is shown that the mechanical properties of LaB_6 should be improved by growing directionally solidified eutectics of the systems LaB_6–MeB_2 (Me–Ti, Zr, Hf). The best mechanical properties were obtained for LaB_6–ZrB_2 directionally solidified eutectics. Also because the refractory borides interact with most metals in the melt, so crucible mold materials have not been found suitable to contain the melt without contamination, the floating zone method appears to have an advantage for the synthesis of these composites [2,4,7].

Because of the high melting point, these composites may also be used as a good structural material at elevated temperatures. At present oxide directionally solidified eutectics have received the most recent attention in this field because they have demonstrated excellent strength and creep resistance up to high-temperatures (>1200 °C), which makes them attractive as high-temperature structural materials [6,9–14]. But this class of materials has low fracture toughness because the interfaces between the two phases typically adopt low-energy orientation relationships during the directional solidification process, which promotes strong bonding and prevents interface debonding [15].

The high-temperature bending strength is one of the main parameters used to evaluate the mechanical properties of structural materials. In most of the previous studies of LaB_6-based ceramics, it was investigated at room temperature [7,8,16], and the crack deflection and bridging are shown as the main toughening mechanisms for the directionally solidified boride eutectics. However, at high temperature, the toughening mechanisms in ceramic materials usually involve changes [9,17,18]. In previous studies [17,18], the authors showed that the high-temperature bending strength of the directionally solidified LaB_6–TiB_2 eutectics depends on the crystallographic orientation of the LaB_6 matrix phase and plasticity of the matrix and fibers. Particularly, in the temperature range of 1000–1600 °C, the highest strength (470 MPa) was observed for the composite grown with the LaB_6 matrix phase ⟨1 0 0⟩ orientation and the lowest strength (350 MPa) for the composite with the ⟨1 1 0⟩ orientation. This dependence was explained by the mutual orientation of the planes of the easiest dislocation glide in the body-centered cubic lattice of LaB_6 and in the hexagonal lattice of TiB_2.

* Corresponding author at: National Technical University of Ukraine "KPI", Peremogy av. 37, Kyiv 03056, Ukraine. Tel.: +380 44 406 82 15;
fax: +380 44 406 82 15.
E-mail address: ubohomol@iff-kpi.kiev.ua (I. Bogomol).

0925-8388/$ – see front matter © 2011 Elsevier B.V. All rights reserved.
doi:10.1016/j.jallcom.2011.02.176

Table 1
The elastic modulus, E, Poisson's coefficient, ν, and linear thermal expansion coefficient, α, of the phases in the binary eutectic used in the self-consistent simulations [23–25].

Phase	E (GPa)	ν	α ($K^{-1} \times 10^{-6}$)
LaB_6	376	0.0386	6.4
ZrB_2	506	0.135	6.9

Therefore, in this study, we investigated the bending strength and toughening mechanisms of the directionally solidified LaB_6–ZrB_2 eutectic composite grown with the ⟨1 0 0⟩ orientation of the matrix phase in the temperature range of 25–1600 °C.

2. Experimental details

Directionally solidified LaB_6–ZrB_2 eutectic composites were obtained by an original floating zone method based on crucible-free zone melting of compacted powders [7,19].

Commercial LaB_6 and ZrB_2 powders (purity 98 wt%, average grain size 1 μm, Reaktiv Co Donetsk, Ukraine) were mixed according to ratios: 79 wt% LaB_6–21 wt% ZrB_2, in accordance with phase diagrams [20]. One volume percent of boron powder (purity 99.8 wt%, particle size 0.5 μm) was added as the impurity solvent. It allows to densify compacted powders to nonporous condition before melting during zone melting [7]. The powders were mixed by sifting them 7 times through a 50 μm mesh. Polyvinyl alcohol was added as a plasticizer. Green rods with a diameter of 10 mm and length of 145 mm were obtained by compressing the mixture in a hydraulic press at 50 MPa. They were dried in a vacuum oven for 12 h at 100 °C and then, placed in the crystal-growth setup "Crystal 206" (Russia), equipped with an induction-type heater. An appropriate LaB_6 monocrystalline seed with crystallographic orientations ⟨1 0 0⟩ was added to obtain monocrystalline samples. Zone melting was carried out in helium atmosphere at excess pressure of 1 atm. The growth rate was fixed at 5 mm/min.

For analysis, the composite samples were cut into rectangular 2.5 mm × 3 mm × 20 mm blocks by a spark-erosive cutter. Their lateral surfaces were ground and polished using diamond pastes. The microstructure and fracture surface of the directionally solidified LaB_6–ZrB_2 eutectic composites were studied using a scanning electron microscopes (SEM) "JEOL JSM-7001F" (Japan) and "Hitachi S4800" (Japan), equipped with an energy-dispersive X-ray spectrometer (EDS). The latter allows mapping the elemental composition inside SEM. Also characterization of the fracture surface was done by transmission electron microscopy (TEM) "Selmi ПЭМ 125К" (Ukraine).

The thermal residual stresses generated upon cooling were computed using the self-consistent model [21,22]. All the phases (LaB_6 and ZrB_2) in the eutectic composite were assumed to be perfectly bonded and embedded in an effective medium, whose properties are precisely those of the composite which are sought. The thermal residual stress tensor in phase i, σ_i, as a result of a homogeneous temperature change ΔT from the stress-free temperature is given by:

$$\sigma_i = b_i \ \Delta T \tag{1}$$

where b_i is the thermal stress concentration tensor of phase i, which is computed as:

$$b_i = (I - B_i)[(C^{-1} - C_i^{-1})^{-1}(a_i - a)] \tag{2}$$

in which I is the unit tensor of fourth order, and a_i and C_i stand for the thermal expansion coefficient tensor and the elastic stiffness tensor of phase i. Assuming that all the phases behaved as isotropic thermo-elastic solids, these tensors are respectively functions of the longitudinal thermal expansion coefficient and of two independent elastic constants, which are given in Table 1. The remaining tensors in Eq. (2) are the mechanical stress concentration tensor of phase i, B_i, and the thermal expansion tensor and the elastic stiffness tensor of the eutectic composite, a and C, which are given by the self-consistent model as:

$$\begin{aligned} B_i &= (C_i[I + (S_i C^{-1})(C_i - C)]^{-1})C^{-1} \\ C &= \sum f_i C_i [I + (S_i C^{-1})(C_i - C)]^{-1} \\ a &= \sum f_i B_i a_i \end{aligned} \tag{3}$$

in which f_i is the volume fraction of phase i and S_i stands for Eshelby's tensor, which depends on the phase shape. The stress-free temperature was taken as 1493 K (ΔT = 1200 K).

The Vickers hardness was measured following the ASTM C1327–99 Standard using a Matsuzawa MMT-7 microhardness tester. The specimens were loaded with 2 N for 15 s, and at least ten valid microindentations were made in each sample. The size of the indentation mark as well as the length of the cracks emanating from the indentation corners was measured immediately after each indentation. The fracture toughness on the transverse cross-section was computed from the Vickers hardness, using the expression proposed by Shetty for Palmqvist cracks [26]. It should be noted that this technique was developed for homogeneous materials and only provides an approximate value for the toughness.

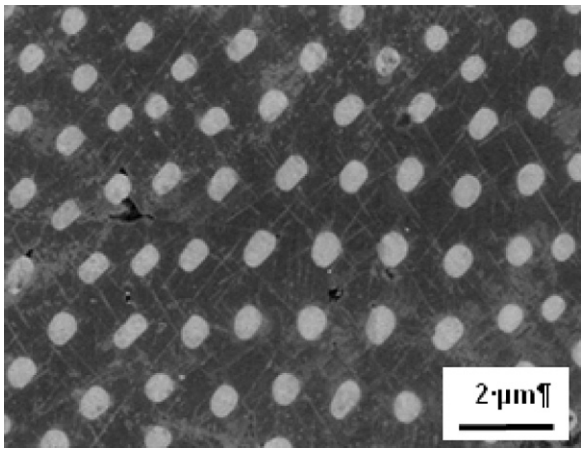

Fig. 1. The cross-section microstructure of the directionally reinforced LaB_6–ZrB_2 eutectic composite.

The three-point bending strength tests were conducted at temperatures of 25, 200, 400, 600, 800, 1000, 1200, 1400 and 1600 °C, in vacuum 1.3×10^{-3} Pa, using an "Instron 4505" setup (USA). The specimens were placed into graphite containers on the SiC supports spaced by 16 mm span. The graphite containers were chambered on the turn table of the testing machine. After evacuation, specimens were fed, by turn, into heating area for bending strength test operation. The loading speed was 0.5 mm/min. Four to six samples were tested at each temperature and the measurement accuracy was taken as the standard deviation.

3. Results and discussion

3.1. Microstructure and elemental analysis

The directionally solidified LaB_6–ZrB_2 eutectic alloy consists of a lanthanum hexaboride matrix reinforced by zirconium diboride fibers oriented along the growth direction (Fig. 1). The average fiber diameter and interfiber spacing are 0.4 and 0.6 μm, respectively. Thus the average eutectic domain size is 1 μm.

An SEM–EDS analysis of a polished surface of the directionally solidified LaB_6–ZrB_2 eutectic composite revealed that it consists of a LaB_6 matrix reinforced with ZrB_2 fibers (Fig. 2(a)). A representative EDS spectrum (Fig. 2(b)) shows B peaks at high energies and a strong signal originating from the Zr and La.

3.2. Residual stresses

For investigation of the toughening mechanisms of the directionally solidified eutectic composite in a wide temperature range, we need to analyze the main factors influencing the mechanical behavior of this type of material under different conditions. There are residual stresses, fracture toughness and the presence or absence of plastic deformation during the loading and fracture of the ceramic composite materials.

The appearance of defects in directionally solidified eutectics should be caused by thermal strains induced by a thermal expansion mismatch between the phases. During cooling of the material from melting, these strains cannot be relaxed because plastic deformation in the ceramics is limited, giving rise to large thermal residual stresses. The observed crack propagation modes will be correlated to the internal stress calculations [27]. In ceramic eutectics, residual internal stresses measurements have already been performed using either X-ray [28,29] or neutron [30] diffraction techniques and Raman spectroscopy [31,32]. These residual stresses significantly affect the mechanical behavior of the material. Concerning the crack propagation modes, tensile stresses within

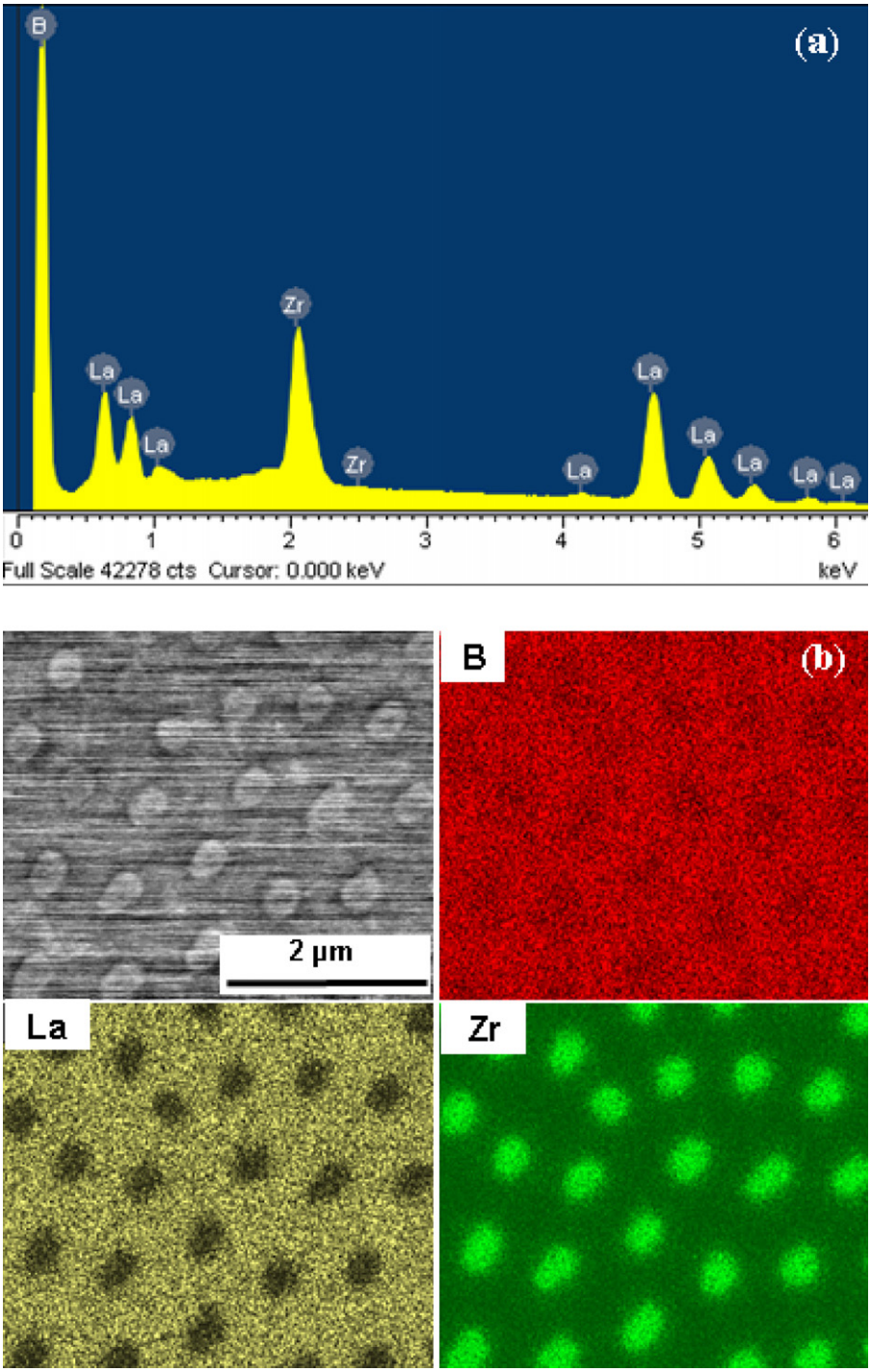

Fig. 2. EDS spectra (a) and mapping (b) of the directionally solidified LaB_6–ZrB_2 composite.

a phase will act in favor of transverse crack propagation in this phase, whereas a normal tensile stress on the phase boundaries will help the interface crack propagation. However, calculation of the internal thermal stresses requires prior knowledge about the thermomechanical parameters of the various phases and the eutectic composites [27].

The accurate estimation of the thermal residual stresses is an important and complex problem, which depends not only on the thermal expansion mismatch, but also on the cooling rate from the eutectic temperature, the morphology of the eutectic microstructure and the development of stress relaxation mechanisms. Although the tensile residual stresses can induce microcracking throughout the directionally solidified eutectics upon cooling [13], their effects are not always undesirable, and controlled residual stresses in composite materials should be used to increase the toughness by enhancing the crack deflection at the interface [11].

In this paper, the residual thermal stresses are computed using a self-consistent approximation for a two-phase composite [21,22]. The self-consistent model assumes that the two phases are columnar grains oriented along the growth direction and forming an entangled network in the perpendicular cross-section, and that the thermal residual stresses arise as a result of the mismatch in their thermo-elastic constants from a stress-free temperature. The average thermal residual stresses in the perpendicular cross-section

Table 2
Thermo-elastic residual stresses at ambient temperature (as computed from the self-consistent approximation) in the LaB_6 and ZrB_2 phases in the perpendicular cross-section.

Phase	$\alpha_\perp$ (MPa)
LaB_6	−121.65
ZrB_2	−23.46

are shown in Table 2. These calculations show that both the LaB_6 and ZrB_2 phases are under compressive stresses. It should promote crack deflection in the directionally solidified LaB_6–ZrB_2 eutectic composite at ambient temperature. Especially, crack deflection is a well-known toughening mechanism in ceramics with columnar or lamellar structures [11,33,34].

3.3. Fracture toughness

In this study the fracture toughness of the directionally solidified LaB_6–ZrB_2 eutectic alloy was also investigated. It is shown that the fibrillar morphology generated by directional solidification led to a significant improvement in the fracture resistance perpendicular to the domains. Cracks parallel to the eutectic domains were nucleated from the corners of the Vickers indentations on the transverse cross-sections (Fig. 3(a)). The fracture pattern showed symmetric, well-defined cracks, and a fracture toughness of 8.9 MPa $m^{1/2}$ was estimated from the length of the cracks [26]. Similar indentations carried out on the longitudinal cross-sections led to an asymmetric crack pattern, in which cracks perpendicular to the single crystal domains were difficult to grow and tended to propagate parallel to them (Fig. 3(b)). These observations have revealed that crack deflection and bridging toughening mechanisms determine the fracture toughness of the directionally solidified LaB_6–ZrB_2 eutectic alloy. It is well-known that the crack deflection in fiber-reinforced or laminated ceramics is achieved through weak fiber–matrix interfaces or through phase with a low toughness [35]. In our case, the fracture toughness of lanthanum hexaboride does not exceed 3.42 MPa $m^{1/2}$ [25].

3.4. Temperature dependence of bending strength

For analysis of the toughening mechanisms at elevated temperatures, the bending strength of the directionally solidified LaB_6–ZrB_2 eutectic alloy was investigated in the temperature range of 25–1600 °C. Fig. 4 shows the bending strength values as a function of temperature. The highest strength (950 MPa) is observed at the temperature of 1600 °C.

Fig. 5(a) and (b) shows the directionally solidified LaB_6–ZrB_2 samples after fracturing at room temperature and 1600 °C, respectively, demonstrating that the roughness of the fractured surface decreases with the increasing testing temperature. Thus, we postulate that at elevated temperatures, the bridging toughening mechanism has not appeared and the crack propagates along the planes of dislocation gliding in the matrix, and the fibers are pulled out or broken.

At higher resolutions, crack deflection and bridging are observed for the samples tested at ambient temperature (Fig. 6(a)). Increasing the testing temperatures leads to the appearance of fibers pulling out of the matrix and to changes in the microstructure of the fracture surface (Figs. 6(b) and (c)). The mechanism by which the fibers are pulled out from the matrix significantly depends on the matrix–fiber interface strength and perfection. Therefore, estimation of the mode of deformation of each phase during testing is very important. It is mainly determined by the thermal residual stresses. At room temperature, the internal compressive stresses in the directionally reinforced LaB_6–ZrB_2 composite characterize the strength because of crack deflection and bridging toughening mechanisms. At elevated temperatures, these stresses are decreased, and the fibers are more often pulled out from the fracture surface (Fig. 6(b) and (c)). At the same time, the experimental data indicate the increasing bending strength of the LaB_6–ZrB_2 eutectic with temperature (Fig. 4) due to the increasing matrix and fiber plasticity. It allows the fracture mechanism from brittle to ductile mode does gradually change.

The increasing matrix and fiber plasticity is observed by investigation of the fracture surfaces of samples tested in the temperature range of 25–1600 °C (Figs. 6–8) and the load–displacement curves (Fig. 9).

The isolated neck formations and holes in the LaB_6 matrix shown in the SEM micrograph of the LaB_6–ZrB_2 surface already fractured at room temperature (Figs. 6(a) and 7(a)) indicate that the plastic deformation of the ZrB_2 fibers occurs before the fracture. At the same time, the samples are fractured by a pure brittle mechanism (Fig. 9). Increasing the testing temperature to 1000 °C leads to an increase in the number of necks on the fiber surface and holes in the matrix (Fig. 6(b)). The load–displacement curve also shows the brittle fracture of the samples (Fig. 9).

At a testing temperature of 1200–1400 °C, slip lines are also observed on the fracture surface of the LaB_6 matrix phase (Fig. 6(c))

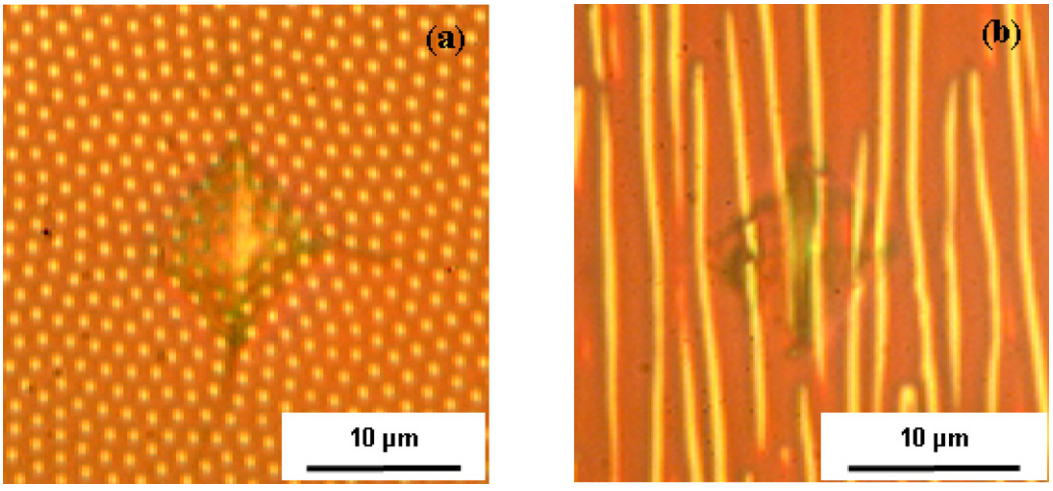

Fig. 3. Cracks generated from the corners of Vickers indentations on polished cross-sections of the directionally solidified LaB_6–ZrB_2 composite: (a) transverse section and (b) longitudinal cross-section.

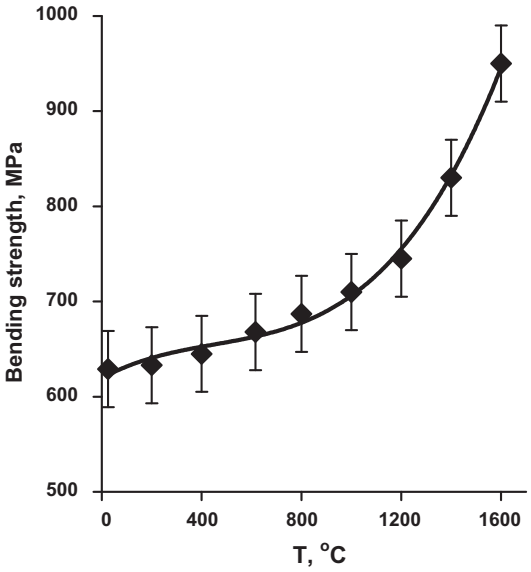

Fig. 4. Temperature dependence of bending strength of the directionally solidified LaB_6–ZrB_2 composite.

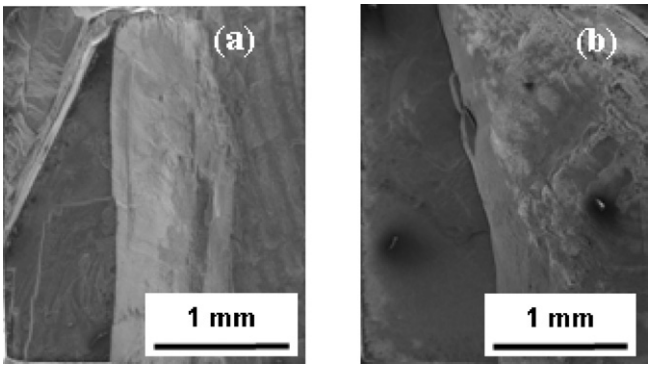

Fig. 5. Macrographs of fractures of the directionally solidified LaB_6–ZrB_2 eutectic alloy at testing temperatures of (a) 25 °C and (b) 1600 °C.

and on the side face of the holes that appeared after pulling out of the ZrB_2 fibers (Fig. 7(b)), although the mode of the load–displacement curves remains typical for the brittle mechanism of fracture (Fig. 9).

The investigation of the fracture surface of the samples tested at 1400 °C by TEM shows that the dislocation arrangement appears in the single crystalline ZrB_2 fibers (Fig. 8(a)). The strained fibers can be divided into regions with different directions of dislocation lines. This picture can signify the strain hardening in single crystalline zirconium diboride fibers during high-temperature deformation which promotes the increasing bending strength values of the directionally solidified LaB_6–ZrB_2 eutectic alloy. This behavior of the fibers confirms the results obtained by authors in a previous study [17] in which strain hardening was discovered in the single crystalline titanium diboride fibers during high-temperature deformation.

At a testing temperature of 1600 °C, a significant plasticity both in the LaB_6 matrix phase and ZrB_2 fibers is observed on the fracture surface of the directionally solidified LaB_6–ZrB_2 eutectic alloy (Figs. 6(d), 7(c) and (d)). Moreover, in contrast to the bending strength tests of this composite at all the other temperatures, the pulling out of the fibers from matrix at 1600 °C is not fixed. These

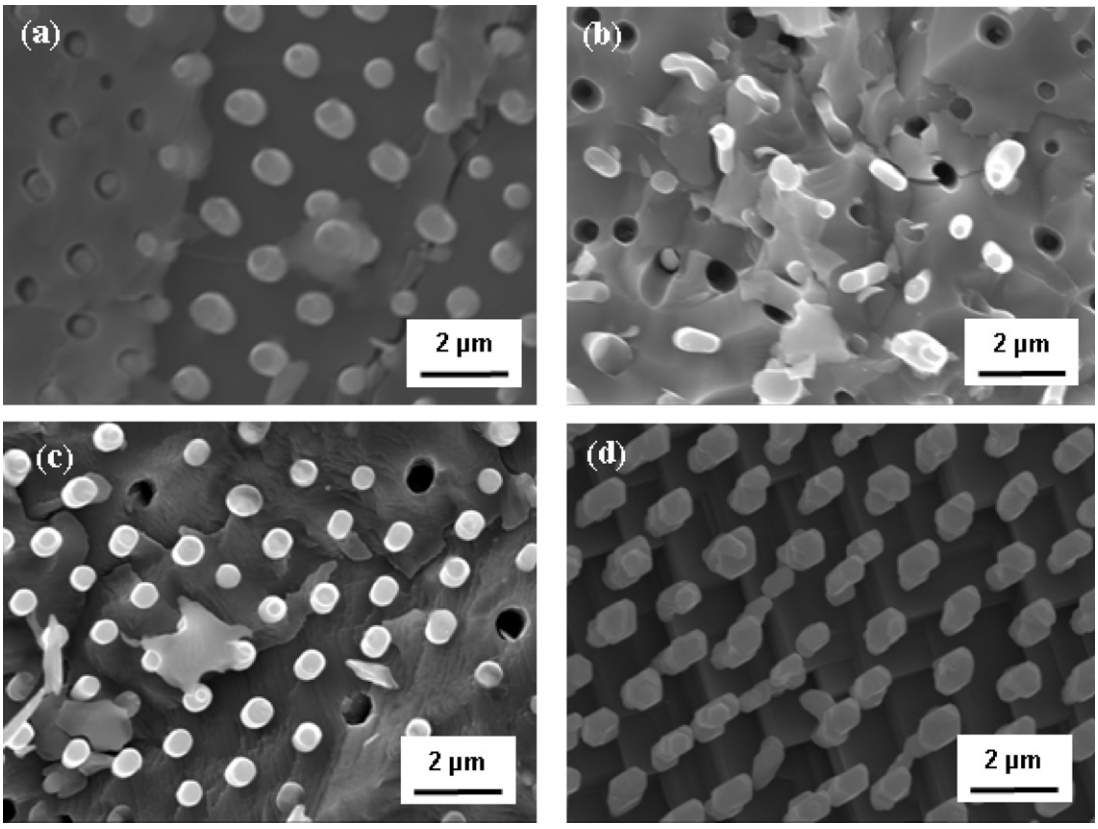

Fig. 6. Micrographs of fractures of the directionally solidified LaB_6–ZrB_2 composite at testing temperatures of (a) 25 °C; (b) 1000 °C; (c) 1400 °C and (d) 1600 °C.

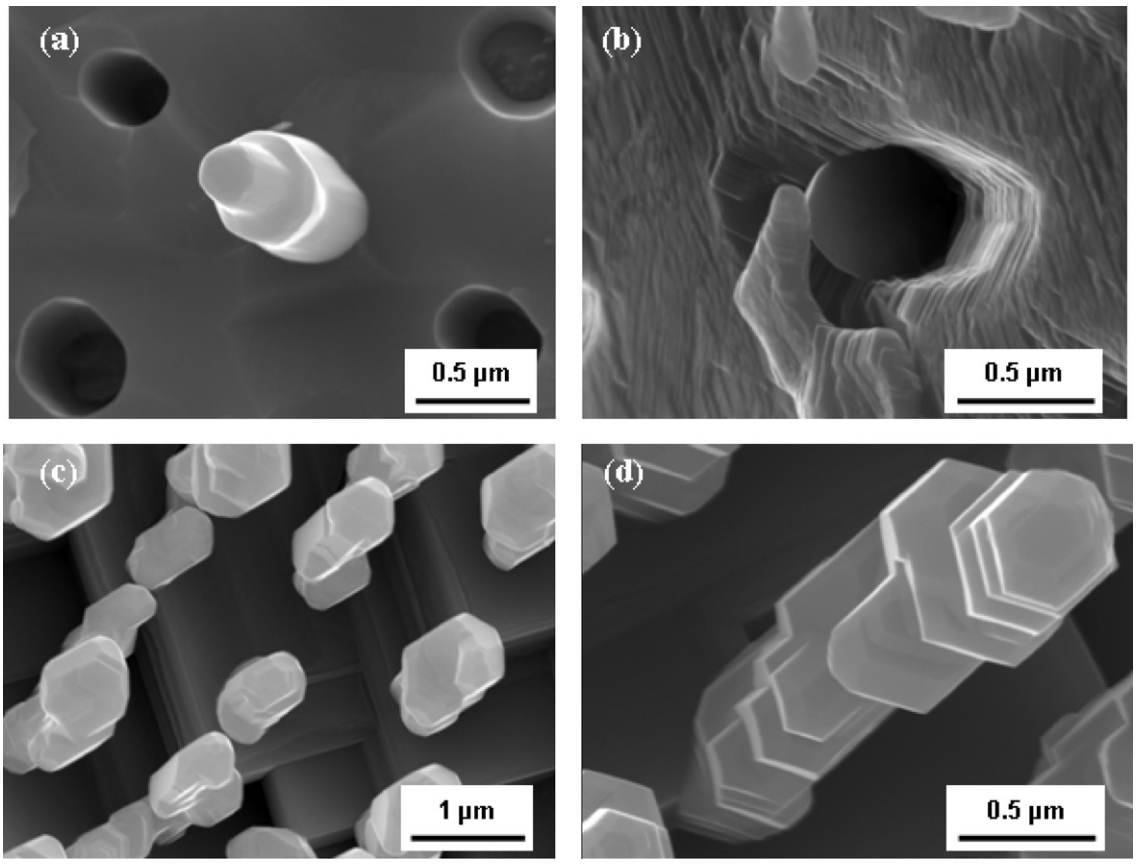

Fig. 7. Micrographs of fractures of the directionally solidified LaB_6–ZrB_2 composite at testing temperatures of (a) 25 °C; (b) 1400 °C; (c) and (d) 1600 °C.

facts could indicate the increasing bonding forces between the matrix and fibers and about the development of stress relaxation processes result in the increasing bending strength of the composite at these temperatures (Fig. 4).

The plastic deformation of the LaB_6 matrix phase appeared in many slip lines with a regular squared shape on the fracture surface (Fig. 7(c) and (d)). These lines correspond to the crystallographic direction ⟨0 0 1⟩ of the LaB_6 body-centered cubic lattice and indicate a significant dislocation motion by the easiest gliding systems [36]. Also, the investigation of the fracture surface of the samples tested at 1600 °C by TEM shows that the dislocation arrangement appears in the LaB_6 matrix (Fig. 8(b)).

The plasticity of the ZrB_2 fibers appeared in the presence of jogs with a regular hexagon shape on the fiber surface (Figs. 7(c) and (d)). These jogs correspond to the basis crystallographic plane ⟨0 0 0 1⟩ of the ZrB_2 close-packed hexagonal lattice and indicate a significant dislocation motion by the easiest gliding systems [36].

The mode of the load–displacement curve for the samples tested at 1600 °C also confirms the occurrence of plastic deformation in the composite (Fig. 9). First, the slope angle of this curve, and

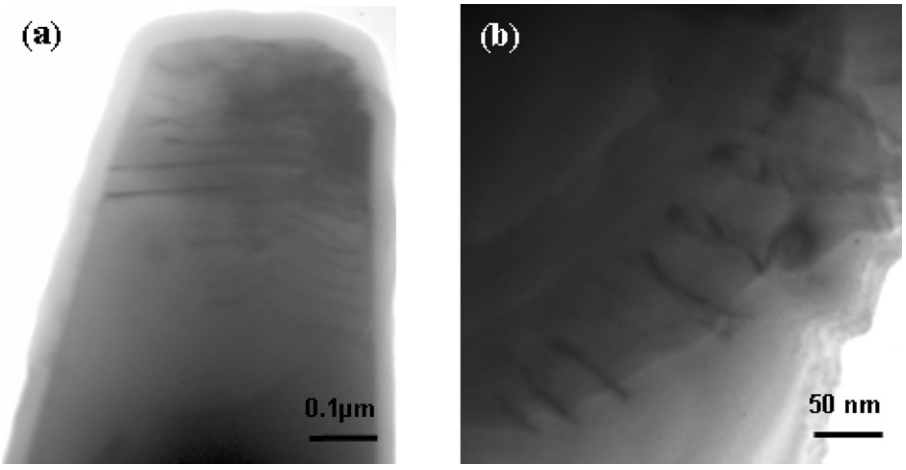

Fig. 8. TEM images of microstructure of strained at 1400 °C (a) ZrB_2 fibers and at 1600 °C LaB_6 matrix (b) in the directionally reinforced LaB_6–ZrB_2 composite.

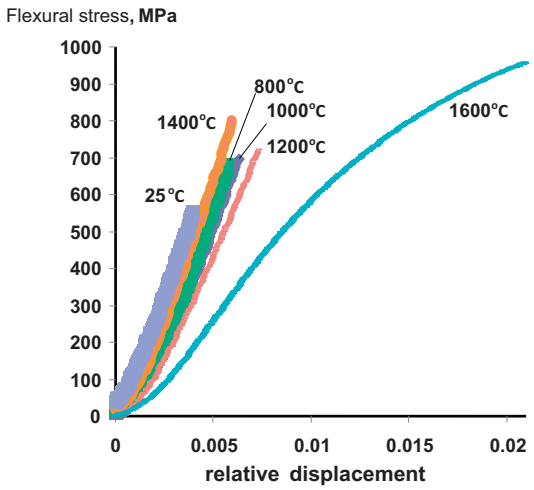

Fig. 9. Typical load–displacement curves for the directionally solidified LaB_6–ZrB_2 composite in temperature range 25–1600 °C.

accordingly Young's modulus, are significantly less than the samples tested at lower temperatures. Secondly, the shape of the curve is typical for plastic deformation. It consists of two regions with different slope angles responding to the elastic and plastic deformations. Thus at a temperature near 1600 °C, the change from the brittle to ductile fracture mode for the directionally solidified LaB_6–ZrB_2 eutectic alloy was revealed.

4. Conclusions

The directionally solidified eutectic LaB_6–ZrB_2 composite with the ⟨1 0 0⟩ direction of the LaB_6 matrix was produced by the floating zone method based on the crucible-free zone melting of the compacted powders. The bending strength of the composite changed with the increasing temperature in the range of 25–1600 °C and reached 950 MPa at 1600 °C. The composite strength in the temperature interval from 25 to 1200 °C is associated with crack deflection, bridging toughening mechanisms and increasing plasticity of the ZrB_2 phase; and at 1200–1600 °C, with the increasing plasticity of the matrix and fibers and strain hardening of the single crystalline ZrB_2 whiskers. The analysis of the load–displacement curves enabled us to determine the change from the brittle to ductile fracture mode for the directionally solidified LaB_6–ZrB_2 eutectic near 1600 °C.

References

[1] H. Hagiwara, H. Hiraoka, R. Terasaki, M. Ishii, R. Shimizu, Scan. Electron Microsc. 2 (1982) 473–483.
[2] V.N. Paderno, Y.B. Paderno, A.N. Pilyankevich, J. Less-Common Met. 67 (1979) 431–436.
[3] M. Mushiaki, K. Akaishi, T. Mori, Mater. Sci. Eng. A 163 (1993) 177–179.
[4] M. Nakamoto, K. Fukuda, Appl. Surf. Sci. 202 (2002) 289–294.
[5] G. Min, R. Gao, H. Yu, J. Han, Key Eng. Mater. 297–300 (2005) 1630–1638.
[6] R.L. Ashbrook, J. Am. Ceram. Soc. 60 (9–10) (1977) 428–435.
[7] P.I. Loboda, Powder Metall. Met. Ceram. 39 (9–10) (2000) 480–486.
[8] H. Deng, E.C. Dickey, Y. Paderno, V. Paderno, V. Filippov, A. Sayir, J. Mater. Sci. 39 (19) (2004) 5987–5994.
[9] Y. Waku, N. Nakagawa, T. Wakamoto, H. Ohtsubo, K. Shimizu, Y. Kohtoku, Nature 389 (1997) 49–52.
[10] K. Hirano, J. Eur. Ceram. Soc. 25 (2005) 1191–1199.
[11] J. Llorca, V.M. Orera, Prog. Mater. Sci. 51 (2006) 711–809.
[12] J. Yi, A.S. Argon, A. Sayir, Mater. Sci. Eng. A 421 (2006) 86–102.
[13] P.L. Kennard, R.C. Bradt, V.S. Stubican, J. Am. Ceram. Soc. 59 (3–4) (1976) 160–163.
[14] C. Oelgardt, J. Anderson, J.G. Heinrich, G.L. Messing, J. Eur. Ceram. Soc. 30 (2010) 649–656.
[15] E.C Dickey, V.P. Dravid, P.D. Nellist, D.J. Wallis, S.J. Pennycook, Acta Mater. 46 (5) (1998) 1801–1816.
[16] Yu. Paderno, V. Paderno, V. Filippov, J. Solid State Chem. 154 (1) (2000) 165–167.
[17] I. Bogomol, T. Nishimura, O. Vasylkiv, Y. Sakka, P. Loboda, J. Alloys Compd. 505 (1) (2010) 130–134.
[18] I. Bogomol, T. Nishimura, O. Vasylkiv, Y. Sakka, P. Loboda, J. Alloys Compd. 485 (1–2) (2009) 677–681.
[19] I. Bogomol, O. Vasylkiv, Y. Sakka, P. Loboda, J. Alloys Compd. 490 (1–2) (2010) 557–561.
[20] P. Loboda, I. Bogomol, M. Sysoev, G. Kysla, J. Superhard Mater. (translation of Rus: Sverkhtverdye Materialy) 28 (5) (2006) 28–32.
[21] Y. Benveniste, G.J. Dvorak, T. Chen, J. Mech. Phys. Solids 39 (7) (1991) 927–946.
[22] R. Hill, J. Mech. Phys. Solids 13 (1965) 213–222.
[23] W. Martienssen, H. Warlimont (Eds.), Springer Handbook of Condensed Matter and Materials Data, Springer, Heidelberg, Berlin, 2005.
[24] N.L. Okamoto, M. Kusakari, K. Tanaka, H. Inui, S. Otani, Acta Mater. 58 (2010) 76–84.
[25] P.I Loboda, H.P. Kysla, S.M. Dub, O.P. Karasevs'ka, Mater. Sci. 45 (1) (2009) 108–113.
[26] D.K. Shetty, I.G. Wright, P.N. Mincer, A.H. Clauer, J. Mater. Sci. 20 (1985) 1873–1882.
[27] L. Perri'ere, R. Valle, L. Mazerolles, M. Parlier, J. Eur. Ceram. Soc. 28 (2008) 2337–2343.
[28] E.C. Dickey, C.S. Frazer, T.R. Watkins, C.R. Hubbard, J. Eur. Ceram. Soc. 19 (1999) 2503–2509.
[29] H. Suzuki, K. Akita, Y. Yoshioka, Y. Waku, H. Misawa, J. Soc. Mater. Sci. Jpn. 52 (2003) 770–775.
[30] S. Torii, T. Kamiyama, K. Oikawa, Y. Waku, T. Fukunaga, J. Eur. Ceram. Soc. 25 (2005) 1307–1311.
[31] G. Gouadec, Ph. Colomban, N. Piquet, M.F. Trichet, L. Mazerolles, J. Eur. Ceram. Soc. 25 (2005) 1447–1453.
[32] J.I. Peña, M. Larson, R.I. Merino, I. de Francisco, V.M. Orera, J. Llorca, et al., J. Eur. Ceram. Soc. 26 (2006) 3113–3121.
[33] J. Llorca, R.N. Singh, J. Am. Ceram. Soc. 74 (11) (1991) 2882–2890.
[34] W.J. Clegg, Science 286 (5442) (1999) 1097–1099.
[35] P.B. Oliete, J.I. Pena, A. Larrea, V.M. Orera, J. Llorca, J.Y. Pastor, A. Martin, J. Segurado, Adv. Mater. 19 (2007) 2313–2318.
[36] D. Hull, D.J. Bacon, Introduction to Dislocations, 4th ed., Butterworth, London, 2001.